Absence of Superconductivity in the Pure Two-Dimensional Hubbard Model

Mingpu Qin,[1,2,*] Chia-Min Chung,[3,4,*] Hao Shi,[5] Ettore Vitali,[6,2] Claudius Hubig,[7] Ulrich Schollwöck,[3,4] Steven R. White,[8] and Shiwei Zhang[5,2]

(Simons Collaboration on the Many-Electron Problem)

[1]*Key Laboratory of Artificial Structures and Quantum Control, School of Physics and Astronomy, Shanghai Jiao Tong University, Shanghai 200240, China*
[2]*Department of Physics, College of William and Mary, Williamsburg, Virginia 23187, USA*
[3]*Arnold Sommerfeld Center for Theoretical Physics, Ludwig-Maximilians-Universität München, 80333 Munich, Germany*
[4]*Munich Center for Quantum Science and Technology (MCQST), 80799 Munich, Germany*
[5]*Center for Computational Quantum Physics, Flatiron Institute, New York, New York 10010, USA*
[6]*Department of Physics, California State University Fresno, Fresno, California 93740, USA*
[7]*Max-Planck-Institute for Quantum Optics, 85748 Garching, Germany*
[8]*Department of Physics and Astronomy, University of California, Irvine, California 92697, USA*

(Received 6 November 2019; revised 27 April 2020; accepted 19 May 2020; published 21 July 2020)

We study the superconducting pairing correlations in the ground state of the doped Hubbard model—in its original form without hopping beyond nearest neighbor or other perturbing parameters—in two dimensions at intermediate to strong coupling and near optimal doping. The nature of such correlations has been a central question ever since the discovery of cuprate high-temperature superconductors. Despite unprecedented effort and tremendous progress in understanding the properties of this fundamental model, a definitive answer to whether the ground state is superconducting in the parameter regime most relevant to cuprates has proved exceedingly difficult to establish. In this work, we employ two complementary, state-of-the-art, many-body computational methods—constrained-path (CP) auxiliary-field quantum Monte Carlo (AFQMC) and density matrix renormalization group (DMRG) methods—deploying the most recent algorithmic advances in each. Systematic and detailed comparisons between the two methods are performed. The DMRG is extremely reliable on small width cylinders, where we use it to validate the AFQMC. The AFQMC is then used to study wide systems as well as fully periodic systems, to establish that we have reached the thermodynamic limit. The ground state is found to be nonsuperconducting in the moderate to strong coupling regime in the vicinity of optimal hole doping.

DOI: 10.1103/PhysRevX.10.031016

Subject Areas: Condensed Matter Physics, Superconductivity

I. INTRODUCTION

Understanding high-temperature superconductivity in the cuprates [1] has been a long-standing mystery and one of the greatest challenges in theoretical condensed matter physics [2]. Very early on, the single-band two-dimensional (2D) Hubbard model [3], along with its cousin, the t-J model, were argued to be the paradigmatic models for this problem [4,5], and in many ways, this suggestion has proven to be accurate. Many of the properties of the cuprates seem to be reasonably well described—or at least mirrored—in the Hubbard model, such as antiferromagnetism [6–8] and its abrupt disappearance upon doping, pairing, and stripe formation, and pseudogap physics [9]. Pairing, when it occurs, can be seen as a consequence of a sort of frustration between the hopping or kinetic energy of the holes and antiferromagnetic correlations, which are disrupted by the hopping.

Superconducting long-range order itself, however, is one of the most delicate properties in these systems. Superconductivity appears to have a subtle competition and coexistence with stripe formation [10–12]. In terms of the models, this means that accurate answers about a possible superconducting phase require simulations that are able to describe all of the possible phases in an unbiased fashion so that their competition can be resolved. One also needs a systematic approach to the zero-temperature as well

[*]These two authors contributed equally to this work.

as the thermodynamic limit, particularly since stripes can introduce a new length scale somewhat larger than the size of a pair. Numerous studies over the years have addressed pairing order in the Hubbard model. They have often been driven by remarkable methodological advances and have led to a great deal of insight in the physics of the model (see, for example, Refs. [13–38]). However, given the competing energy scales and intertwined states, it can reasonably be argued that none has satisfied these rigorous criteria for establishing the nature of superconductivity in the physically relevant parameter regime. Both positive and negative results have been found for d-wave pairing order, reflecting the extreme sensitivity of the ground state and low-lying excitations in the model, and the competition between d-wave and other states [33,39–54].

The relation between superconductivity and stripes or other orders is also strongly affected by modifications of the model, such as the next-nearest-neighbor hopping t'. Given the existence of superconductivity in the cuprates with an apparent electronic mechanism, it seems likely that some modification of the pure model exhibits superconductivity. For example, recent studies on width-four cylinders—where DMRG can be pushed to resolve the competing phases to high accuracy—found a nonsuperconducting filled-stripe state in the pure model but quasi-long-range pairing correlations with the addition of a t' term, coexisting with half-filled stripes [38,55–57]. While superconductivity arising from the addition of a t' is encouraging, one clearly needs to go beyond width four. (Note that a width-four cylinder is equivalent to a stack of plaquettes, and there is no difference between a pair on a plaquette and a half-filled stripe. Larger systems are needed to properly allow stripes and superconductivity to compete or coexist.) Hopping parameters t' and third neighbor (diagonal) t'' have been predicted using electronic structure methods [58]; however, even small differences in these parameters can alter the ground-state phase, and it is difficult to establish whether additional terms, such as hopping mediated by a second hole, are important. It is also not clear whether one needs to study a three-band model in order to connect directly with the cuprates.

Here, we choose to focus on the pure Hubbard model, with parameters U and t only. The existence or absence of superconducting order in this fundamental model at moderate to strong coupling is an outstanding theoretical question. This question has presented a 30-year challenge, magnified by the quest to understand high-T_c superconductivity. An intense experimental effort is ongoing with ultracold atoms in optical lattices to realize "quantum simulations" of this model [59–62]. The model has also served as a barometer for the capacity of the computational physics and chemistry community to perform reliable computations in interacting quantum systems. We study pairing correlations and superconductivity using two complementary methods—the density matrix renormalization group (DMRG) and auxiliary-field quantum Monte Carlo (AFQMC) methods. Our work follows up on a previous study involving four different methods that determined that the ground state of the Hubbard model has stripe order at $1/8$ doping [63]. Although stripes may tend to compete with superconductivity [64], it may be possible for them to coexist [12,34,65–68].

The constrained-path AFQMC method [69,70] we use treats the fermion sign problem approximately, so validation is important. Here, we use DMRG [71] on width-four and width-six cylinders to validate an approach to predict pairing orders in AFQMC. The DMRG calculations involve multiple independent DMRG programs pushed to the limit of current capabilities. We find excellent agreement between the DMRG and AFQMC. The AFQMC does not have DMRG's width restrictions, and we then use the AFQMC to study systems of over 250 lattice sites, including periodic boundary conditions. In the AFQMC calculations, we devise new techniques to probe the superconducting order, both through a linear response measure of the order parameter and through the use of a BCS trial wave function to directly measure the pairing correlation function. These simulations allow us to conclude that only short-range pairing occurs in the regime of interest (U/t around 6–8 and dopings $0.1 < h < 0.2$), and the system is not superconducting.

In the small U/t limit, controlled results from perturbation theory have shown that the Hubbard model has a superconducting ground state [72–75]. Diagrammatic Monte Carlo studies [76] indicate that a BCS superconducting state of d-wave symmetry can emerge at weak coupling ($U/t < 4$) for doping $h \geq \sim 0.3$. Given the sensitive and delicate nature of the ground state of the model, and, in particular, given that stripe formation is believed not to occur at weak coupling [75], it is very interesting how this part of the phase diagram connects with the other parameter regimes. We emphasize that our work does not imply a general statement that there is no superconducting order anywhere in the pure Hubbard model. Rather, our focus is on the nature of the pairing order in the pure Hubbard model in the physically important parameter regime as a model for cuprate superconductors.

The rest of this paper is organized as follows. Section II discusses the two different methods we employ and two different ways in each to probe pairing and superconducting order. Our results are presented in Sec. III: first, a general scan of the doping dependence of the superconducting order at $U = 8$; then, a detailed study of the case of $U = 8$ and $h = 1/8$, followed by an analysis of the relation between pairing and stripe order; and next, the dependence on the interaction strength. We conclude in Sec. IV. Further technical details as well as additional results are included in the Appendixes.

II. APPROACH

We study the pure Hubbard Hamiltonian with nearest-neighbor hopping and on-site interaction:

$$\hat{H} = -t\sum_{\langle ij\rangle\sigma}\hat{c}^{\dagger}_{i\sigma}\hat{c}_{j\sigma} + U\sum_{i}\hat{n}_{i\uparrow}\hat{n}_{i\downarrow} - \mu\sum_{i\sigma}\hat{n}_{i\sigma}, \qquad (1)$$

where $\hat{c}_{i\sigma}$ is the fermionic annihilation operator, σ denotes spin ($=\uparrow$ or $\downarrow$), $\hat{n}_{i\sigma} = \hat{c}^{\dagger}_{i\sigma}\hat{c}_{i\sigma}$ is the particle number operator on site i, and $\langle ij\rangle$ denotes nearest neighbor sites. We study rectangular lattices of size $N = L_x \times L_y$, typically with periodic boundary conditions (PBC) along the y direction and open boundary conditions along the x direction (i.e., cylinder geometry). We vary the aspect ratios of the cylinders (e.g., 32×8, 24×14) to ensure that the rectangular cells do not impact our results [77]. We perform finite-size extrapolations. Additionally, we perform complementary calculations with PBCs along both directions. We set t as the energy unit, i.e., $t = 1$.

We denote the number of electrons in the simulation cell by N_e, with $N_e = N_\uparrow + N_\downarrow$. The electron density or filling factor is $n = N_e/N$, and the hole doping level is then $h = 1 - n$. These quantities are specified in an average sense, as N_e is controlled by the chemical potential μ and will fluctuate in most of our calculations.

A. Two complementary methods

In this work we employ two state-of-the-art methods, constrained-path (CP) AFQMC and DMRG. These methods are representative of the leading edge of computational capabilities for interacting quantum many-fermion systems. They involve very different approximations in obtaining ground-state properties in the thermodynamic limit. To quantify the CP error in AFQMC, we benchmark the results in finite systems of narrow cylinders, where DMRG is highly accurate. The AFQMC does not have size or boundary condition restrictions and can reliably approach the thermodynamic limit. The systematic, detailed, and complementary use of these leading computational techniques is a unique and distinguishing feature of the present study. The excellent agreement between the two methods allows us to draw conclusions with confidence.

1. Constrained-path auxiliary-field quantum Monte Carlo

In AFQMC, the interaction part of the Hamiltonian is recast into a summation (or an integral) of noninteracting terms through a Hubbard-Stratonovich transformation. As a result, physical quantities are represented as a path integral in many-dimensional auxiliary-field space. The high-dimensional summation or integral can be evaluated with Monte Carlo techniques [6]. However, with few exceptions, a minus sign problem is present [78], which causes an exponential growth of the statistical errors with system size. The CP approach overcomes this difficulty by imposing a boundary condition in auxiliary-field space, which is derived from an exact property of the path integral [69] but whose practical implementation involves a trial wave function. The use of CP introduces a systematic error, which can be improved with better trial wave functions. Usually, simple wave functions such as the Hartree-Fock solution have been used as trial wave functions, and previous results [79] show the systematic error is typically small. Recently, we introduced an approach [70] to optimize the trial wave function self-consistently, further reducing the systematic error. As mentioned, a key feature of this work is the combined use of CP-AFQMC with DMRG, which allows us to systematically gauge the accuracy of CP in cylindrical systems.

Ground-state AFQMC is typically formulated in a sector of the Hilbert space with a fixed number of particles, N_e, and fixed S^z (although a corresponding approach in Hartree-Fock-Bogoliubov space exists [80]). Our computation of the pair-pair correlation function is done in this manner, by separate AFQMC calculations on the original Hubbard Hamiltonian in Eq. (1), using backpropagation [69] and BCS trial wave functions [81]. In this work, the order parameter is computed in AFQMC after a particle-hole transformation has been applied to Eq. (1), which results in a modified Hamiltonian that conserves the total particle number [36] but breaks total S^z (further details are given in Appendix A). As described in the next section, in this formulation, the order parameter can be computed from total energy calculations, which leads to very accurate results.

2. Density matrix renormalization group

DMRG is a variational method [71,82] that can be understood in the language of matrix product states (MPS) [83]. The MPS matrix dimensions, or the so-called bond dimensions, indicate the number of states kept in the reduced Hilbert space and play central roles in the approximation. A general many-body state can be represented by a MPS with exponential growth of the bond dimension from the edges. In practice, one restricts the maximum value of the bond dimension, thus limiting the maximum entanglement allowed in the variational state. Ground states of local Hamiltonians of physical interest generally have low entanglement. DMRG minimizes the energy in this low-entanglement Hilbert space. The accuracy of DMRG can be systematically improved by increasing the bond dimension. Although DMRG is naturally formulated and most powerful for one-dimensional systems, it is now widely applied to 2D systems [84] and remains one of the most accurate numerical methods in 2D.

In this work, we employ two DMRG schemes with different conserved quantum numbers, using different update schemes. The first scheme conserves only the S^z_{tot} with $U(1)$ symmetry and uses the two-site update in the

optimization. This scheme is used when a pairing field is applied to the system, breaking the particle number conservation. In such systems, the particle numbers are controlled by the chemical potential. This scheme efficiently enables fluctuations between different quantum numbers in the optimization and is less likely to be stuck in a local minimum. The truncation errors in this scheme are on the order of 10^{-7} (smaller doping) to 10^{-5} (larger doping). The second scheme [85] conserves both the $U(1)$ total particle number and $SU(2)$ spin symmetries and uses the single-site update [86,87]. The single-site update is faster than the two-site update and thus allows us to achieve large bond dimension. This scheme is used for systems without pairing fields, which thus conserve total particle number. Since the truncation error is ill defined in the single-site update, we use the two-site energy variance in the standard extrapolations [88]. The number of states kept in these systems is up to 30 000 $SU(2)$ states, which corresponds to about 90 000 $U(1)$ states, providing the best accuracy attained to date, to our knowledge.

B. Two different ways to characterize superconducting correlation

To study the superconducting properties in the ground state, we use two different probes: pair-pair correlation functions and the pairing order parameter. These probes are both defined in terms of the pairing operator of a pair of nearest-neighbor sites, i and j:

$$\hat{\Delta}_{ij} \equiv \frac{(\hat{c}_{i\uparrow}\hat{c}_{j\downarrow} - \hat{c}_{i\downarrow}\hat{c}_{j\uparrow})}{\sqrt{2}}. \tag{2}$$

We compute the pair-pair correlation function

$$P_{i'j',ij} = \langle \hat{\Delta}^{\dagger}_{i'j'}\hat{\Delta}_{ij}\rangle \tag{3}$$

and the pairing order parameter

$$\Delta_{i,j} = \langle(\hat{\Delta}_{ij} + \hat{\Delta}^{\dagger}_{ij})/2\rangle, \tag{4}$$

where $\langle\cdots\rangle$ denotes expectation with respect to the many-body ground state.

The pair-pair correlation function in Eq. (3) can be obtained directly in a calculation working in a sector with fixed particle numbers. From this function, the d-wave pairing correlation function, $P^d(i-i')$, can be constructed as a function of pair separation $(i'-i)$, by considering all j in $\langle ij\rangle$ and all j' in $\langle i'j'\rangle$, following the sign convention for d-wave as we specify next.

The pairing order parameter in Eq. (4), on the other hand, requires a different approach. We add a term in the Hamiltonian describing SC pairing fields [77,89] applied to the system:

$$\hat{H}_p = -\sum_{\langle i,j\rangle} h_p^{ij}\frac{\hat{\Delta}_{ij} + \hat{\Delta}^{\dagger}_{ij}}{2}, \tag{5}$$

where the amplitude of h_p^{ij} is given by the parameter h_p, and the sign of h_p^{ij} is positive if the bond (i,j) is vertical (along the $\hat{y}$ direction) and negative otherwise (along the $\hat{x}$ direction), in order to probe pairing order of the structure $d_{x^2-y^2}$ [90,91].

In AFQMC, we can obtain the superconducting pairing order parameter Δ from total energy calculations, using the Hellmann-Feynman theorem:

$$\Delta(h_p) \equiv \left\langle \frac{d(\hat{H}+\hat{H}_p)}{dh_p}\right\rangle_{|\Psi_0(h_p)\rangle} = \left.\frac{dE(h_p)}{dh_p}\right|_{h_p}, \tag{6}$$

where $|\Psi_0(h_p)\rangle$ and $E(h_p)$ are the ground-state wave function and energy of the Hamiltonian $(\hat{H}+\hat{H}_p)$. We compute the derivative in Eq. (6) by the finite difference $\Delta(h_p) = (E(h_p-\delta) - E(h_p+\delta)/2\delta) + \mathcal{O}(\delta^2)$, where δ is chosen to be sufficiently small to ensure that the error is smaller than our statistical error bar or targeted resolution. As $h_p \to 0$, the order parameter in the unperturbed ground state is obtained. This approach allows us to directly compute the pairing order parameter in AFQMC, which had not been possible before.

We next use an example to illustrate the above approach to compute order parameters. We consider the antiferromagnetic (AFM) Neel order at half-filling. A staggered inducing field is applied to the periodic supercell of size $L_x = L_y = L$, with magnitude h_m and alternating signs on the two sublattices. Because of the absence of the sign problem at half-filling, no constraint is needed in the AFQMC calculation, and the results are exact numerically. In Fig. 1(a), we show the computed staggered AFM order parameter $M_L(h_m)$ as a function of the applied field strength h_m for different lattice sizes. Extrapolation to the thermodynamic limit (TDL) is then performed at each fixed h_m, as illustrated in panel (b). The resulting TDL values are plotted in panel (c) versus h_m and extrapolated to the $h_m \to 0$ limit to obtain the order parameter. The result of 0.236(3) is in excellent agreement with the previous result of 0.236(1) computed from spin-spin correlation functions [92]. This test provides a validation of our approach for computing superconducting order parameters, which follows identical procedures. (We note that the staggered AFM magnetization in the repulsive Hubbard model at half-filling can be mapped to the s-wave on-site pairing order parameter in the attractive Hubbard model, through a partial particle hole transformation as discussed in Appendix A.)

In the following two subsections, we show benchmark results on the two ways to compute the pairing order, respectively. Careful and detailed comparisons are made

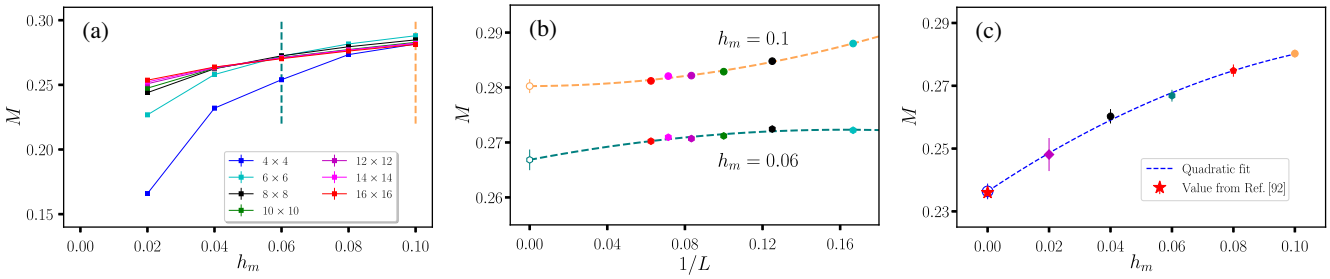

FIG. 1. Illustration of the approach to compute order parameters. The AFM order parameter at half-filling ($U = 4$) is computed by applying staggered magnetic fields to the periodic supercell. (a) The computed magnetic order parameter M is shown as a function of the pinning field strength h_m for different system sizes. (b) A quadratic fit is performed at each h_m to extrapolate $M(h_m)$ to the TDL. The procedure is shown for two values $h_m = 0.06$ and 0.1, as marked by the vertical dashed lines in panel (a). (c) An extrapolation of $M_\infty(h_m)$ to the $h_m \to 0$ limit is then performed, again using a quadratic fit. The resulting $M_\infty(0)$ is shown by the open symbol. The value is in excellent agreement with the order parameter determined from direct computation of spin-spin correlation functions [92], shown by the red star.

between AFQMC and DMRG, first for computing the pairing order parameter and then for pair-pair correlation functions, by using cylindrical geometries. Our results after applying these approaches to address the physical properties of the Hubbard model are presented in Sec. III.

1. Pairing order parameter

The ground-state energies of 16×2 and 16×4 systems computed from AFQMC and DMRG are shown in the top panel of Fig. 2, as a function of the applied pairing field strength h_p. Uniform "d-wave" pairing fields are applied to the entire system. A fixed value of μ is used, which gives a doping of $1/8$ at $h_p = 0$ ($\mu = 1.75$ for 16×4 and $\mu = 1.55$ for 16×2). In AFQMC, the trial wave functions are optimized self-consistently by coupling to natural orbitals [70]. (For small h_p, the resulting trial wave function is the same as the noninteracting wave function.) The inset shows the difference between the energies computed from AFQMC and DMRG. The relative error of the AFQMC energy is less than 0.5% for all h_p in Fig. 2, which means the CP error is very small.

In the bottom panel of Fig. 2, we plot the pairing order parameters from AFQMC and DMRG, for the same system. In DMRG, the order parameter is directly computed as a ground-state expectation value for each h_p, while in AFQMC, it is computed with the approach involving Hellman-Feynman theorem described above. Agreement between the two methods is excellent throughout the entire range. The general behavior of the order parameter is similar to that of the AFM order in Fig. 1 for small supercell sizes. The pairing order parameter approaches 0 linearly as $h_p \to 0$, which is reasonable as spontaneous symmetry breaking can only occur in the TDL. At small h_p, a rapid drop is seen in Δ, deviating from the trend at larger h_p. The behavior is also manifested in the energy results, as we show in Appendix B: A fit of the energies at $h_p > h_p^{\mathrm{th}}$ (where h_p^{th} is a threshold whose precise value does not affect the result) gives an $E_{\mathrm{SC}}(h_p = 0)$ that lies above the true ground-state energy of the system.

We also show the comparison for the pairing order parameter at $U = 4$ and $h = 1/6$ in a 24×4 cylinder, in

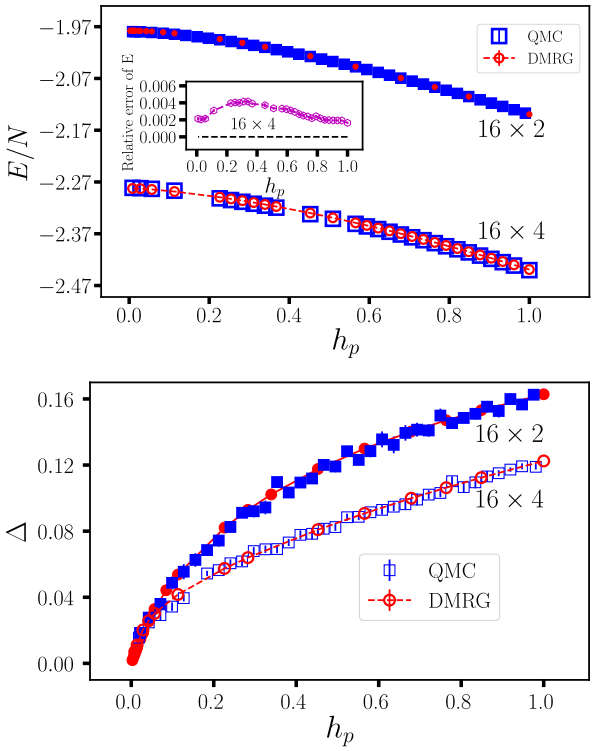

FIG. 2. Upper panel: Comparison of the ground-state energies computed from AFQMC (blue) and DMRG (red), as a function of the applied pairing field strength h_p, at $U = 8$. Two cylindrical systems are shown, 16×2 and 16×4, with the chemical potential held fixed in each so that the doping is $1/8$ when $h_p \to 0$. The inset shows the difference of the energy computed from AFQMC with respect to DMRG. Lower panel: Comparison of the computed SC pairing order parameter for the same systems.

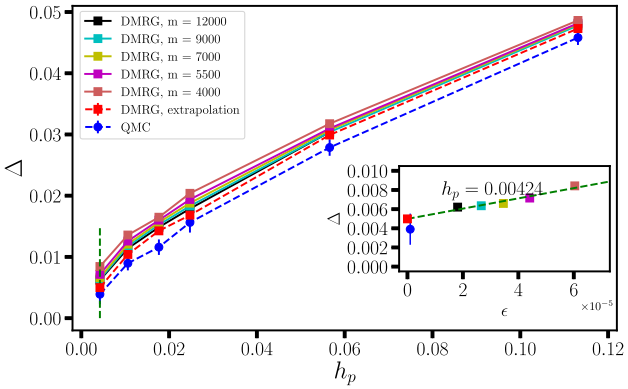

FIG. 3. Comparison of the computed pairing order parameter at $U = 4$, as a function of the applied pairing field strength h_p. The system is a 24×4 cylinder, at $h \simeq 1/6$. DMRG results, with $U(1)$ symmetry and a two-site update, with different bond dimensions are shown. The results after extrapolation to zero truncation error are also plotted. The inset illustrates the extrapolation (with respect to the truncation error) at $h_p = 0.003 \times \sqrt{2} \approx 0.00424$. The red dot represents the extrapolated value from DMRG, while the blue dot with the error bar is the AFQMC result.

Fig. 3. Noninteracting trial wave functions are used in the calculation. Note that the pinning field range here is much smaller than in Fig. 2, focusing on the weak fields and a very fine scale of the pairing order parameter for comparison. With the lower value of U, this system requires larger bond dimensions in DMRG to converge, and we illustrate the extrapolation with truncation error. Good agreement is seen in the order parameters computed from AFMQC and the extrapolated results from DMRG.

2. Pair-pair correlation function

The pair-pair correlation function is computed with a fixed number of particles (canonical ensemble). Results from CP-AFQMC have been obtained earlier in supercells with PBC using free-electron trial wave functions [35] and also using a BCS type of trial wave function after a particle-hole transformation [36]. Here, we employ a more direct and general approach to apply projected BCS trial wave functions [81], and we are able to access much larger systems because of algorithmic improvements and especially increased computing power. Our results are consistent with the earlier studies [35,36]. More unique to this work is the detailed and direct comparison with DMRG to quantify the accuracy.

In Fig. 4, we show a comparison of the pair-pair correlation function for 24×4, at doping of $1/8$, with $U = 4$ in a cylindrical geometry between DMRG and AFQMC. The pair-pair correlations have a much smaller signal (roughly Δ^2), as can be seen even in these small system sizes. Agreement is reasonable, but the accuracy does not reach the level seen with the order parameter calculations. Hence, the order parameter will be the primary tool

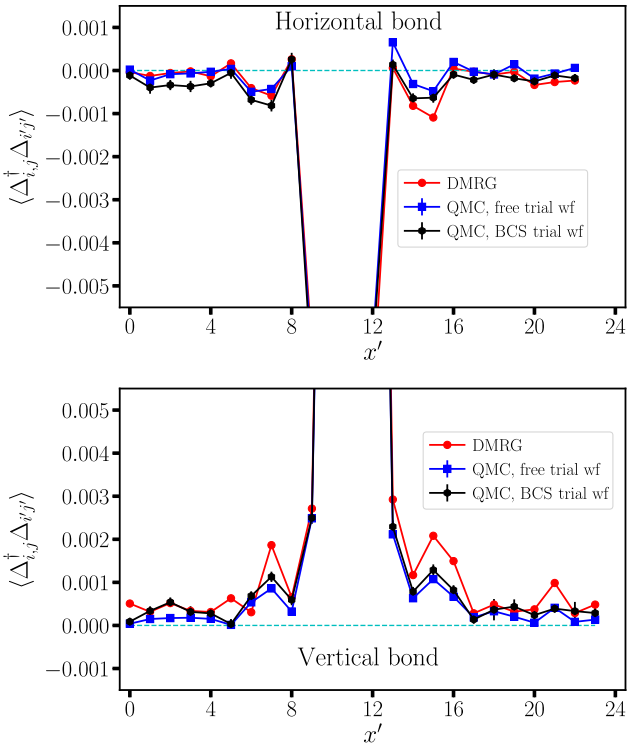

FIG. 4. Comparison between DMRG and AFQMC of the pair-pair correlation function for a 24×4 cylinder, with $U = 4$ at $1/8$ doping. The reference bond is [(12,1), (12,2)]. Vertical and horizontal bonds are along the y and x directions, respectively.

on which we rely to accurately determine the nature of superconducting orders. Thus, the development in this work of direct computation of the order parameter is crucial.

C. Competition between pairing and stripes: Small-cylinder finite-size effects

A central question to this work is how stripe order and pairing order compete or cooperate. The interaction between the two types of order plays out in subtle ways on small-diameter cylinders. In this section, we discuss this interplay in a general, intuitive way, as a guide for the subsequent finite-size scaling analysis.

Let us think about how one can have a striped state that also has pairing order. One would expect that two different requirements should be associated with such a state. The first is that an individual stripe would have local pairing—that one can think of a stripe as being made up of pairs. The second is that, in order to have long-range phase coherence, particularly between stripes, there should be substantial pair tunneling between stripes, associated with a density of off-stripe pairs. One might think of this case as a vapor pressure of pairs outside the "liquid" of stripes. Stripes that bind their pairs too tightly would have weak or nonexistent long-range pairing order. Numerical approaches, in order to probe the 2D thermodynamic limit, must connect to these two requirements.

Previous work on stripes has touched on the local pairing question. Filled stripes were first obtained theoretically in Hartree-Fock calculations, which are based on a single-particle mean-field approximation, without any notion of pairing. If filled stripes have pairing, it would be a subtle modification of the nonpaired mean-field state. In contrast, there is evidence that partially filled stripes have local pairing structure. For example, in DMRG simulations of the t-J and Hubbard models on cylinders, it was noticed that the ring-shaped stripes circling the cylinder strongly favor an even number of holes. For example, on a width-six cylinder, one finds stripes with either four or six holes, not three or five. Another example is shown in Appendix C. In DMRG simulations without particle-number conservation, the hole number in a stripe is always even as the chemical potential is varied.

To study whether pairs can leave their stripes, it is essential that the pair and the stripe are distinct. On a two-leg ladder, there are only pairs, so one cannot address this question. On a width-four cylinder, a half-filled stripe is a pair, so one cannot expect to probe the 2D physics very well on this system. A four-hole filled stripe on a width-four cylinder would allow probing of pairs leaving the stripe, but because the stripe is filled, it may not support pairs within the stripe. Thus, the smallest cylinder that can address both key questions has width six, where one can have a four-hole stripe circling the cylinder.

Note that width-four cylinders have another complication, unrelated to the thermodynamic limit. As discussed for the case of the t-J model [93], there are two very distinct forms of d-wave pairing on a width-four cylinder. One is the usual type, living on the surface of the cylinder. The unusual type forms pairs circling the cylinder, for which it is useful to think of the cylinder as a stack of plaquettes. It has been known for some time that a single plaquette nicely fits a d-wave pair. This state seems especially 1D-like. Note that next-nearest-neighbor hopping t' connects sites within pairs for the surface pairing state but not for the plaquette state.

III. RESULTS

This section contains the following four parts. We first scan the pairing susceptibility versus doping h at a representative interaction strength of $U = 8$. We then carry out a detailed and systematic study of the pairing properties at $1/8$ and $U = 8$ in Sec. III B. This section is followed by an examination of the relation between stripe and SC orders in Sec. III C and then an investigation of the dependence on U in Sec. III D.

A. d-wave pairing susceptibility versus doping

We first probe the SC response as a function of electron density, by computing the pairing order parameter in the presence of a d-wave pairing field, which is applied to the entire system. We choose the pairing field amplitude around $h_p = 0.05$, which induces a sizable SC order but does not drive the system far away from its ground state (see Fig. 15 in Appendix C). The electron density n is controlled by the chemical potential μ. For the 16×4 cylinder, the μ value is varied in the range of 1.4 to 2.0, which yields an electron density from about 0.79 to 1. Figure 5 shows the SC pairing order parameter as a function of density, or doping level. It can be seen from the 16×4 scan that the SC order has a stronger response between $n \sim 0.81$ and 0.92, with the maximum close to $n = 0.885$. Results in wider systems remain consistent, with the SC order showing slow variations in the vicinity of $h = 1/8$ doping. At density near the maximum SC order, the system displays charge and spin orders consistent with the ground state at $1/8$ doping ($n = 0.875$), namely, a stripe order [63]. This result indicates that the system shows a SC order in response to the applied pairing field but remains in a similar ground state as the one when the pairing field is absent.

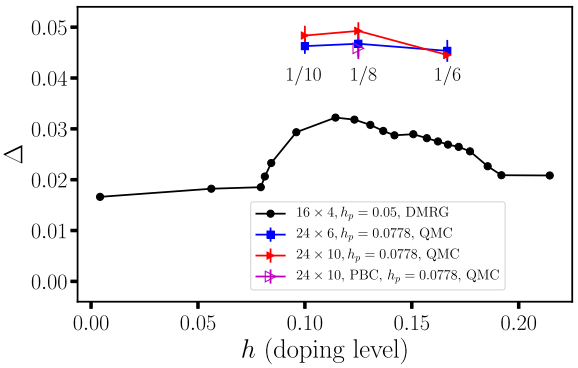

FIG. 5. SC order parameters as a function of doping level, with $U = 8$. Results from three systems are shown, each at a modest value of the applied d-wave pairing field (with strength h_p indicated in the legend). The doping level or particle density is controlled by varying the chemical potential.

We have also investigated the doping dependence of the SC response in a 64×4 system using a different but complementary approach to the one in Fig. 5. A linearly varying chemical potential $\mu(x)$ is applied along the cylinder, and the SC order and local density are computed without a pairing field by allowing particle numbers to fluctuate in the DMRG calculation. The dependence of the SC order as a function of local density is found to be consistent with that in Fig. 5, as shown in Appendix C.

The fact that $1/8$ doping is near the maximum response of the SC order for $U = 8$, and that the SC order shows rather weak dependence on the precise density, leads us to focus on the system of $h = 1/8$, $U = 8$, for which there is also detailed data on the spin and charge order, as well as ground-state energy, to compare with. The interaction strength of $U = 8$ is chosen as representative of the physically relevant regime. The results are presented in the next section.

B. Absence of long-range *d*-wave pairing order at $U=8$ and $h=1/8$

We begin this section by considering a 48×4 cylinder at $h = 1/8$, with a pairing pinning field applied on vertical bonds at the left edge only. We measure how the SC pairing order parameter $\langle \hat{\Delta}_{ij} \rangle$ decays as a function of distance from the left edge, which gives an indication of the behavior of the pairing correlation function in the bulk. We expect at least algebraic decay of the pairing order parameter if the system exhibits long-range SC order and exponential decay if there is no such order. The calculations are done with DMRG, without conserving particle number but with $U(1)$ symmetry for S^z_{tot}. In Fig. 6, we show the SC pairing order parameter on the vertical ($\hat{y}$) bonds along the $\hat{x}$ direction. The SC pairing order parameter is well converged when the bond dimension reaches $m = 12\,000$, so no extrapolation is needed. We perform both exponential and algebraic fits. The SC pairing order parameter clearly decays exponentially versus distance from the pinning field. As shown in the inset in Fig. 6, the pairing order on the horizontal ($\hat{x}$) bonds is perfectly symmetric with the negative values of the vertical bonds. Although the pairing pinning fields are applied only on the vertical bonds at the left edge, the whole system spontaneously builds a *d*-wave pairing structure. This result further confirms the tendency for short-range *d*-wave pairing; however, the exponential decay of the pairing order indicates that there is no long-range SC order in the filled stripes.

We next investigate the pair-pair correlation directly on a 48×6 cylinder. At $h = 1/8$ doping, the ground state has filled stripes with $\lambda = 8$ [63]. Previous study on width-two ladders found that the SC pair-pair correlation decays algebraically [94], while further study on width-four cylinders showed that the correlation decays exponentially [55]. Here, we study a width-six cylinder, employing the $U(1) \times SU(2)$ symmetry adapted DMRG with a single-site update and keeping bond dimension up to 22 000 $SU(2)$, which is, to our knowledge, the largest bond dimension to date in studying the SC pairing on width-six cylinders. The computed SC pair-pair correlation is then extrapolated with respect to the two-site energy variance [88]. (The extrapolation details can be found in Appendix E.) Again, we perform both exponential and algebraic fits. As shown in Fig. 7, the SC pair-pair correlations clearly follow an exponential decay with pair separation, showing no long-range order. The inset shows the (negative) values of the correlations on the vertical (horizontal) bonds. The correlations on the horizontal bonds are perfectly symmetric with the vertical bonds but with opposite sign, again confirming the *d*-wave structure.

On the width-six cylinders, in addition to the filled stripes with $\lambda = 8$, the 2/3-filled stripes with $\lambda \approx 5$ can also be stabilized, and this state has a slightly higher energy ($\sim 0.001t$) [63] than the ground state studied above. This state has a wavelength closer to the stripes ($\lambda = 4$) observed experimentally [95], so it is interesting to also investigate the pairing in this metastable state.

Using DMRG, we computed the pair-pair correlation function in 48×6 cylinders at 1/8 hole doping in this state. As in the ground state with filled stripes, the results are shown in Appendix D. The pair-pair correlation is found to

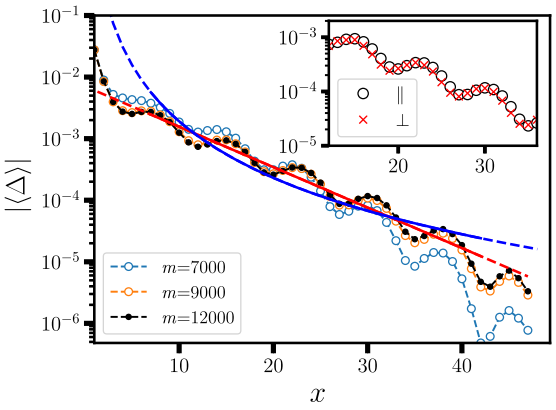

FIG. 6. SC pairing order parameter on the vertical bonds at a fixed y, versus position x, for a 48×4 cylinder at 1/8 hole doping, computed from DMRG with $U(1)$ symmetry (S^z_{tot}) and a two-site update. Pairing fields with $h_p = 0.25$ are applied to the vertical bonds at the left edge $x = 0$. Results with different bond dimension m are shown. Both exponential (red line) and algebraic (blue curve) fits are shown; the solid (dashed) region indicates the region (not) used in the fits. The oscillation of the pairing order parameter coincides with the stripe period. The inset shows the (negative) pairing order parameters on the vertical (∥) [horizontal (⊥)] bonds for $m = 12\,000$.

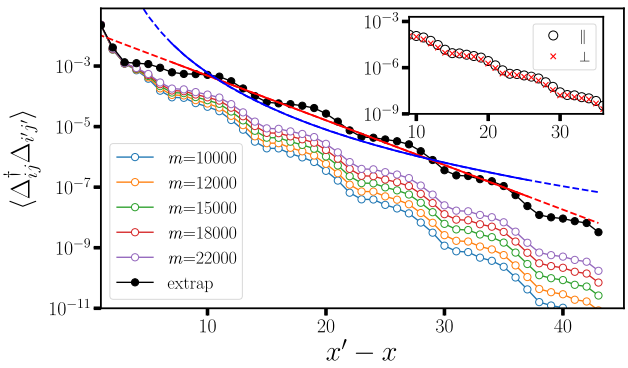

FIG. 7. SC pair-pair correlation on the vertical bonds at a fixed y, versus pair separation, for a 48×6 cylinder at 1/8 hole doping, computed from DMRG with $U(1) \times SU(2)$ symmetry and single-site update. Results of different bond dimensions m, as well as the extrapolation to the infinite bond dimension, are shown. The pair separation $(x' - x)$ is measured with respect to the reference bond, a vertical bond at $x = 5$. Both the exponential (red line) and the algebraic (blue curve) fits are shown; the solid (dashed) region indicates the region (not) used in the fits. The correlation length is approximately 2.9 from the fitting. The inset shows the (negative) correlations on the vertical (∥) [horizontal (⊥)] bonds for $m = 22\,000$.

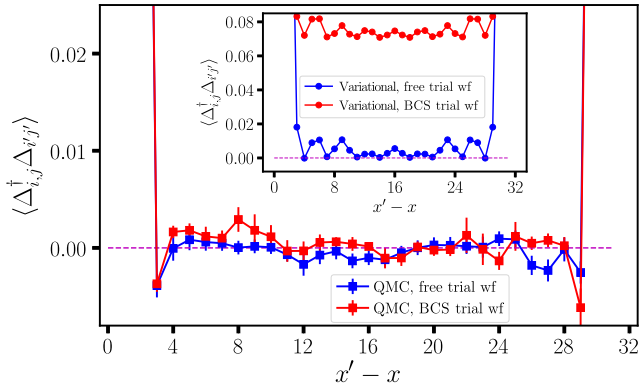

FIG. 8. Pair-pair correlation from QMC for a 32×6 system with $U = 8$, $1/8$ doping and PBC. Different trial wave functions are used. In the inset, the results from trial wave functions themselves are shown. Comparing to the variational result in the BCS wave function, the pair-pair correlation in the QMC calculation, using it as a trial wave function, is largely suppressed.

decay exponentially, even faster than in the ground state with filled stripes.

It is worth emphasizing that we have used two different DMRG schemes above—one under $U(1)$ symmetry (S^z_{tot}) with two-site updates and the other under $SU(2) \times U(1)$ (spin and particle number) with strictly single-site updates. The consistency between the two approaches is a further confirmation of their reliability. The width of the systems that can be studied efficiently with DMRG is limited due to the linear increase of entanglement entropy with the width. To reach the TDL in two dimensions, we complement DMRG with two kinds of AFQMC calculations, computing both the pair-pair correlation function and the pairing order parameter, as described next.

The pair-pair correlation function in an 32×6 supercell with PBC along both directions is shown in Fig. 8. This calculation is performed with a fixed number of electrons, at $h = 1/8$, with $U = 8$. The calculation with a free-electron trial wave function is consistent with earlier results from CP-AFQMC on square lattices [35,36]. The calculation with a number-projected BCS trial wave function, as mentioned, employs a new method [81], which allows direct computation and backpropagation in the Hubbard model working in the canonical ensemble. For both free-electron and BCS trial wave functions, the pair-pair correlations from AFQMC are seen to decay to 0 within the statistical resolution beyond a few lattice spacings. The BCS wave function itself has very large pair-pair correlation, as shown in the inset. However, in the AFQMC result, using it as a trial wave function, the pair-pair correlation is suppressed by 2 orders of magnitude and decays to 0 beyond a few lattice spacings. While the agreement between the two trial wave functions is not perfect, their consistent behavior at large pair separation provides another corroboration of the results from the pairing order parameter.

We next employ AFQMC to calculate the pairing order parameter, by applying $\hat{H}_p$ as in Eq. (5), with the pairing fields chosen to match the $d_{x^2-y^2}$ structure and applied throughout the supercell. The pairing order parameter Δ (averaged over all bonds) is calculated as a function of h_p. The chemical potential $\mu = 1.75$ is chosen such that the hole density is $h = 1/8$ in the ground state when $h_p = 0$, and it is held fixed for all h_p. To detect possible long-range SC pairing order in the pure Hubbard model ($h_p = 0$), we need to reach the TDL at each h_p first and then extrapolate h_p to zero. This procedure is parallel to what is illustrated in Fig. 1, and it is shown in Fig. 9. Following the procedure discussed in Sec. II B, AFMQC calculations are performed on various system sizes up to 32×8. We focus on the small-h_p region where the behavior determines whether long-range SC pairing order exists. In this region, the self-consistent trial wave function gives the same results as the

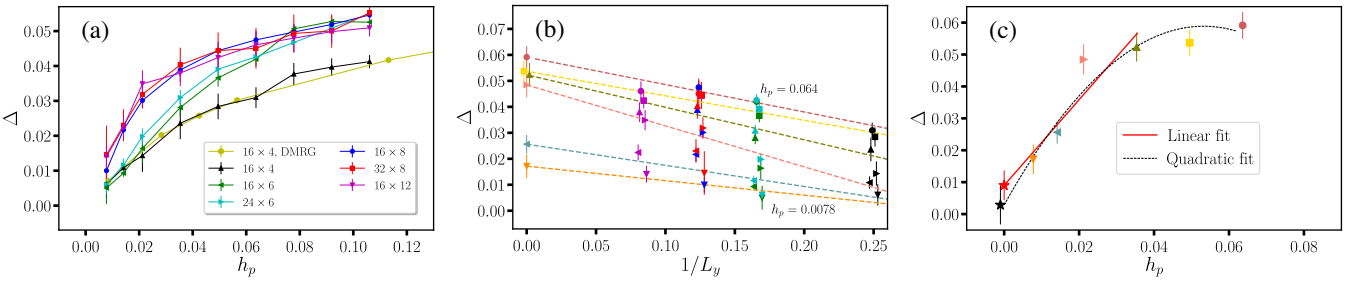

FIG. 9. Finite-size scaling of the SC pairing order parameter, at $U = 8$ and $h = 1/8$. In panel (a), the computed pairing order parameters Δ are shown for a variety of system sizes in the small-h_p region. In panel (b), an extrapolation of the results in panel (a) is performed with respect to the width in the periodic direction (linear in $1/L_y$) for each value of h_p. The lines, from top to bottom, are for $h_p = 0.064, 0.049, 0.035, 0.021, 0.014$, and 0.0078, respectively. The resulting pairing order parameter $\Delta_\infty(h_p)$ is shown on the left. (A slight shift in the horizontal position has been applied to some of the data points for better visibility of the results and error bars.) In panel (c), the result from the fit in panel (b), $\Delta_\infty(h_p)$, is plotted versus h_p. A quadratic fit is then performed, which yields a value $\Delta_\infty(0) = 0.003(6)$, as indicated by the black star at $h_p = 0$. A linear fit of the last few points is also shown. Weighted least-squares fits are used to account for the statistical errors.

noninteracting trial wave function; the latter form is used here, which is obtained by setting $U = 0$ in Eq. (1) and tuning the chemical potential to give a doping of $h = 1/8$. The computed pairing order parameters as a function of h_p are shown in Fig. 9(a). For the lengths studied here ($L_x > 16$), the results are not sensitive to L_x, as can be seen by comparing the 16×6 and 24×6 results, and also the 16×8 and 32×8 results. On the other hand, the order increases when the system becomes wider, although the dependence on system size becomes weak beyond $L_y = 6$. To obtain the order parameters at the TDL, $\Delta_\infty(h_p)$, a linear extrapolation with $1/L_y$ is performed for each value of h_p, as shown in Fig. 9(b). The resulting $\Delta_\infty(h_p)$ and the statistical uncertainties are shown in Fig. 9(c). A quadratic fit is then performed, which yields a value $\Delta_\infty(0) = 0.003(6)$, as indicated by the symbol at $h_p = 0$. A linear fit for $h_p < 0.05$ is also shown, which gives a statistically consistent result. We thus conclude that there is no long-range SC pairing in this system in the TDL.

C. Competition between stripe and superconducting orders

In Fig. 10, we examine the trend of the stripe and SC pairing orders when the strength of the applied pairing field is varied. The stripe order amplitude is defined as the intensity of hole modulation in the stripe state (i.e., the maximum value minus the minimum value of hole density along the longer direction of the cylinder). Results are presented for two systems, a 16×4 cylinder computed by DMRG and a 32×8 cylinder computed by AFQMC. Both results are for $U = 8$, with $h = 1/8$. We can see that, when h_p is decreased, the pairing order parameter becomes smaller while the stripe order increases. The two orders thus compete against each other in the Hubbard model. The results of the previous subsection show that, at the zero pairing field limit, the stripe order dominates and no pairing order survives in this parameter region.

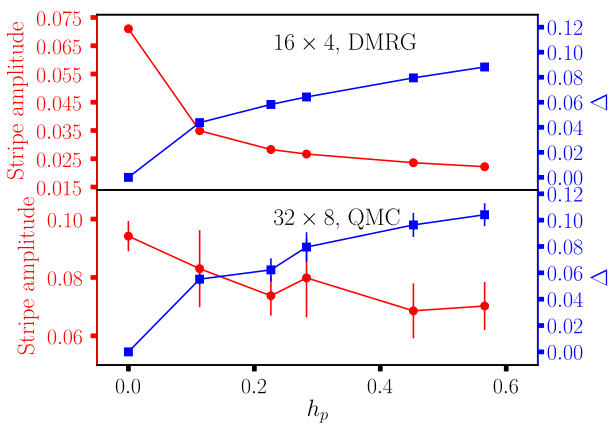

FIG. 10. Strengths of the stripe and pairing orders versus the applied pairing field, h_p. The upper and lower panels show results from 16×4 and 32×8 cylinders, respectively, both at $U = 8$ with $h = 1/8$.

D. U dependence, and the case of $U = 4$

In this section, we study the pairing order at different interaction strengths U. In Fig. 11, we plot the pairing order parameter for $U = 4$, 6, and 8 at $1/8$ doping. These calculations follow the same procedure as in Fig. 2, performed on a 16×4 system, with pairing fields of d-wave structure applied to the entire system. In the large-h_p region, we find that the SC pairing order parameter increases as U decreases. In the small-h_p region, the pairing order parameter varies little with the decrease of U.

Given the tendency for the pairing susceptibility to increase as U is reduced, we next focus on a lower but still physically relevant value of $U = 4$. In Fig. 12, we show the pair-pair correlation function for $1/8$ doping from DMRG. The study at $U = 4$ is similar to the one in Fig. 7 at $U = 8$. Consistent with the result from Sec. III C, the pairing correlation amplitude is substantially larger than for $U = 8$. Both exponential and algebraic fits are performed for the correlation function computed with the largest bond dimension kept, $m = 30\,000$. Here, the results are less definitive. The exponential is a slightly better fit to the data, but the algebraic fit cannot be ruled out conclusively.

We next study the pairing order parameter at $U = 4$, using AFQMC to approach the TDL. We target $h = 1/6$, near optimal doping. In this parameter regime, no stripe or spin-density wave state is observed in the ground state of the Hubbard model [51]. This system is the one in which extensive cross-checks between DMRG and AFQMC were performed in Sec. II B (Fig. 3). The computed pairing order parameters for a variety of system sizes are shown in Fig. 13. The same procedure as in Fig. 9 is performed.

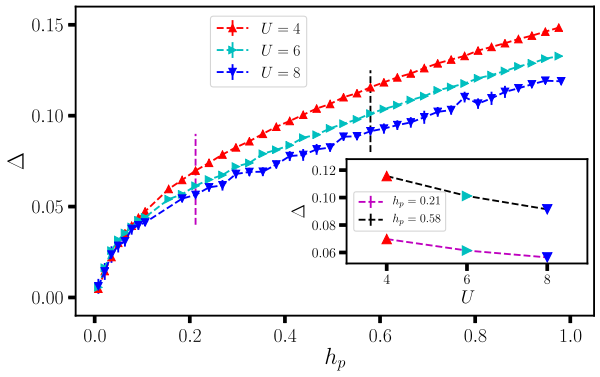

FIG. 11. Dependence of the pairing order parameter on interaction strength U. Calculations were done in the same manner as in Fig. 2, on 16×4 systems, varying only U. In the inset, the pairing order parameters are plotted versus U for two values of h_p as indicated by the vertical lines in the main graph, $h_p = 0.38$ and 0.58.

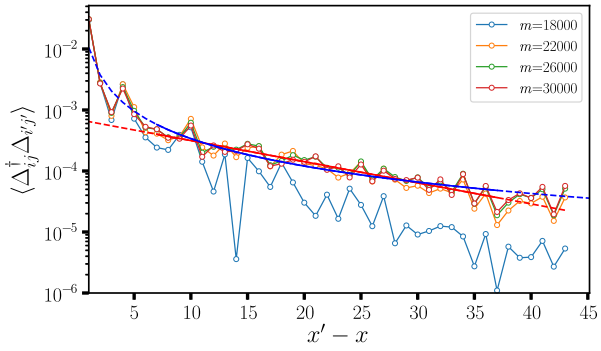

FIG. 12. SC pair-pair correlation on the vertical bonds for $U = 4$ at $h = 1/8$ on a 48×4 cylinder, computed by DMRG with $U(1) \times SU(2)$ symmetry and the single-site update. The reference bond is a vertical bond at $x = 5$. Both exponential (red line) and algebraic (blue curve) fits are shown; the solid (dashed) region indicates the region (not) used in the fits.

We first carry out an extrapolation with the width L_y at each h_p, to reach the TDL. In contrast to the $U = 8$ case, the pairing order parameter here is seen to either decrease or saturate very quickly with system width as L_y grows. The results for width-four cylinders (24×4) are seen to be nonmonotonic with wider systems, so they are not included in the fit. The final result extrapolated to the $h_p = 0$ limit is $\Delta_\infty(0) = 0.006(4)$, statistically compatible with a vanishing order parameter.

Of course, based on this result and the pairing correlation results above, we cannot fully rule out the possibility of a finite pairing order in the ground state at $U = 4$. (See also the discussion on weak coupling in Sec. I.) Our results put a rather stringent bound on the strength of the pairing order, which is considerably smaller than indicated by the best previous calculations with affirmative results on superconductivity. The small magnitude of this bound suggests that, even if the pure Hubbard model is superconducting in some regime of the parameter space further from the most relevant physical parameters, it is likely missing key ingredients as a fundamental model for cuprate superconductors.

IV. SUMMARY AND PERSPECTIVE

In summary, we have carried out a detailed study of the superconducting pairing properties in the ground state of the 2D pure Hubbard model, using two of the most accurate ground-state many-body computational methods available at present. With both methods, we have presented technical advances that enabled new capabilities in probing the superconducting order. The DMRG calculations of pairing correlation functions were performed on up to width-six cylinders, with unprecedented accuracy. For the first time, the AFQMC computations were able to compute pairing order parameters relying on total energy calculations. Meticulous comparisons were made between the two methods. Their complementary application allowed us to maintain high accuracy and reach the thermodynamic limit.

In the parameter regime relevant to the cuprates ($U \sim 6$–8), we found that the pure Hubbard model does not have a superconducting ground state. We also found that the lack of superconductivity is due to a competition with stripe order, with stripes dominating. At smaller $U \sim 4$, the tendency for striped ground states is much weaker. In this case, we still find a pairing response consistent with zero. While we cannot rule out a small nonzero pairing order parameter, our results place an upper bound on its strength, which is very small.

In the early days of high-temperature cuprate superconductivity, when no numerical approach was adequate to accurately probe the low-temperature doped regime in large system sizes, it was natural to expect that if one could get past the fermion sign problem, one would quickly have a clear picture of the physics involved. Now that we can study this regime, new obstacles have been revealed. A key obstacle is the close competition of a number of different phases, with small Hamiltonian terms mediating which phase is favored. This situation makes simulations more difficult, but equally important is that it is very difficult to know reliably which sets of small terms and parameters (such as next-nearest-neighbor hopping t') describe the actual materials. Our work can be viewed as a key initial

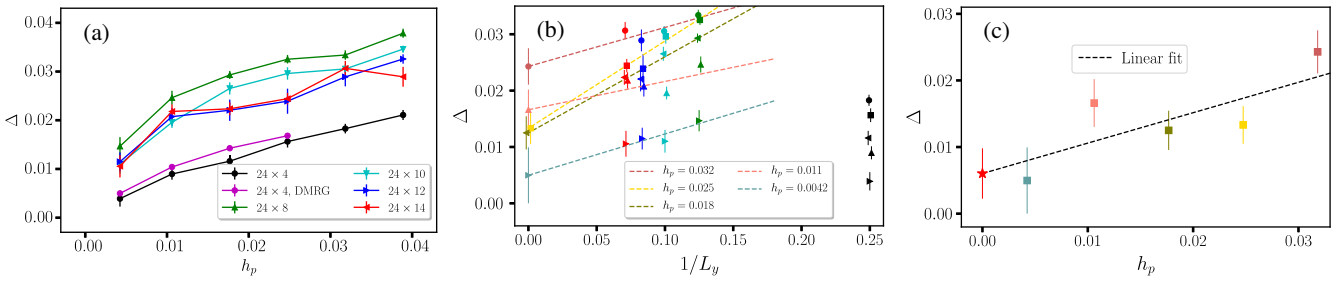

FIG. 13. Finite-size scaling of the SC pairing order parameter, at $U = 4$ and doping of $h \simeq 1/6$. The layout is the same as in Fig. 9. In panel (a), the pairing order parameter computed from DMRG for 24×4 (see Fig. 3) are also shown for comparison. In panel (b), the width-four data (black symbols) were not included in the linear fits, as they are nonmonotonic with larger L_y results. In panel (c), the extrapolation yields a value $\Delta_\infty(0) = 0.006(4)$, as indicated by the symbol at $h_p = 0$.

step, where the iconic simplest-to-define model with only U and t is found not to exhibit superconductivity. To go beyond this step, one can study phases and superconductivity in generalized models, including a broad range of parameters. Simultaneously, it is important to improve our techniques for both deriving accurate models and for simulating real systems with very strong correlation without introducing models.

It is also important to note that the pure Hubbard model does get much of the physics right, including antiferromagnetism and its destruction upon doping, and a tendency for stripes to occur and to compete with d-wave superconductivity. It also produces the crucial physics that there are many intertwined states separated by tiny energy scales, a key part of the reason that the complete nature of superconductivity in the cuprates remains to be resolved.

ACKNOWLEDGMENTS

We acknowledge helpful discussions with E. Gull, M. Imada, and A. J. Millis. M. Q. and S. Z. were supported by the Simons Foundation. The Flatiron Institute is a division of the Simons Foundation. S. R. W. acknowledges the support of the NSF through Grant No. DMR-1812558. C.-M. C. and U.S. acknowledge support by the Deutsche Forschungsgemeinschaft (DFG, German Research Foundation) under Germany's Excellence Strategy 426 EXC-2111 390814868. Parts of the calculations were carried out at the Extreme Science and Engineering Discovery Environment (XSEDE), which is supported by National Science Foundation Grant No. ACI-1053575, and the computational facilities at the College of William and Mary. C. H. acknowledges funding through ERC Grant QUENOCOBA, ERC-2016-ADG (Grant No. 742102).

APPENDIX A: PARTICLE-HOLE TRANSFORMATION

When the pairing fields in Eq. (5) are applied, the Hamiltonian contains fluctuations of the total particle number. The usual ground-state AFQMC is formulated in the canonical ensemble with fixed N_e. However, we can apply a partial particle-hole transformation as follows:

$$\hat{c}_{i\uparrow} \to \hat{d}_{i\uparrow}, \qquad \hat{c}^{\dagger}_{i\uparrow} \to \hat{d}^{\dagger}_{i\uparrow},$$
$$\hat{c}_{i\downarrow} \to \hat{d}^{\dagger}_{i\downarrow}(-1)^i, \qquad \hat{c}^{\dagger}_{i\downarrow} \to \hat{d}_{i\downarrow}(-1)^i. \tag{A1}$$

Then, the Hamiltonian in Eq. (1) is transformed to

$$\hat{H} = -t\sum_{\langle i,j\rangle\sigma}\hat{d}^{\dagger}_{i\sigma}\hat{d}_{j\sigma} + U\sum_i(\hat{m}_{i\uparrow} - \hat{m}_{i\downarrow}\hat{m}_{i\uparrow}) - \mu\sum_i(\hat{m}_{i\uparrow} + 1 - \hat{m}_{i\downarrow}), \tag{A2}$$

where $\hat{m}_{i,\sigma} = \hat{d}^{\dagger}_{i,\sigma}\hat{d}_{i,\sigma}$. The pairing operator in Eq. (5) is transformed from Eq. (2) to $\hat{\Delta}_{ij} = ((-1)^{j+1}\hat{d}^{\dagger}_{j\downarrow}\hat{d}_{i\uparrow} - (-1)^i\hat{d}^{\dagger}_{i\downarrow}\hat{d}_{j\uparrow})/\sqrt{2}$, which now describes spin-flip hopping terms. The chemical potentials for electrons with up and down spin are now $\mu - U$ and $-\mu$, respectively, introducing spin imbalance in the system. The sign of interaction strength U is flipped, which means the interaction becomes attractive after the transformation. In CP-AFQMC calculations, walkers (Slater determinants) are now represented as a $2N \times N_e$ matrix [8], and each orbital in the Slater determinant is now a spin orbital with a mixture of up and down orbitals. This case is similar to the treatment of Hamiltonians with spin-orbit coupling terms [96]. Other details remain unchanged in the CP-AFQMC calculation.

APPENDIX B: COMPARISON OF ENERGIES BETWEEN THE PAIRING STATE AND THE STRIPE STATE

In Fig. 14, we show the comparison of energies between the pairing state and the stripe state. The systems are 16×4 cylinders, with a d-wave pairing field applied to the whole system. The energy for the pairing state at $h_p = 0$ (denoted by triangles in Fig. 14) is obtained from a quadratic fit with energies at large h_p. The stripe energy (denoted by the open square and cycle in Fig. 14) is the actual value calculated at $h_p = 0$. We find that the energy of the pairing state is slightly higher than that of the stripe state, by about 0.01 per site.

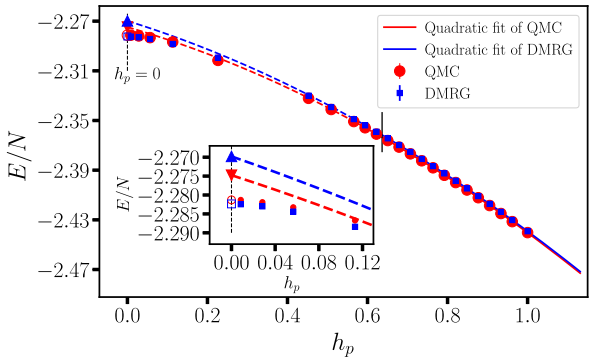

FIG. 14. Comparison of the ground-state energies from CP-AFQMC (red) and DMRG (blue), as a function of the pairing field strength h_p. The system is a 16×4 cylinder. A fixed value of $\mu = 1.75$ is used with which the doping is $1/8$ when $h_p = 0$. A quadratic fit is applied to each set of energies using only values at large h_p (points to the right of the vertical bar). The triangular symbols at $h_p = 0$ show the intercept result from the fit, while the open symbols are those obtained from actual calculations done at $h_p = 0$. In the inset, a zoom of the main plot near $h_p = 0$ is shown.

APPENDIX C: FURTHER INVESTIGATION OF DOPING DEPENDENCE

In the main text, we have shown the pairing order induced by the pairing field $h_p = 0.05$ for different doping in Fig. 5. Here, we illustrate that the pairing field amplitude $h_p = 0.05$ only slightly changes the original ground state, and thus the induced SC order properly represents the response of the original ground state. In Fig. 15, we compare the local hole densities of two 16×4 systems. One is a system with pairing field $h_p = 0.05$ and $\mu = 1.72$, corresponding to overall particle density of approximately 0.872. The other is a system of conserved particle density 0.875 without a pairing field. The stripe order can be clearly seen in both systems, and the pairing fields only slightly change the local densities.

To further examine the doping dependence of the pairing order, we study, using DMRG, a 64×4 cylinder with local chemical potential $\mu(x)$ linearly changing from 1.4 to 2.1 along the longitudinal (x) direction. Since the local density will vary with x, we obtain information about different dopings in a single calculation. We use DMRG *without* conserving total particle number to allow SC orders to develop. The local densities and the local SC orders along the longitudinal direction are shown in Fig. 16. The SC orders on the horizontal and vertical bonds are symmetric with opposite signs, showing the d-wave symmetry. The maximum SC order appears around the density $n \approx 0.875$ (1/8 hole doping), and it decays for both higher and lower densities. This result is further confirmation of the doping dependence of the SC order observed in Sec. III A, and it validates the choice of doping $h \sim 1/8$ as a representative case in studying the SC response.

The optimal doping $\mu_{\text{opt}} \approx 1.73$ is actually at the boundary between two different stripe fillings. For $\mu < \mu_{\text{opt}}$, the ground states are filled stripes (four holes per stripe in the width-four cylinder), and for $\mu > \mu_{\text{opt}}$, the ground states are half-filled stripes (two holes per stripe). This case can be seen from the more abrupt change in density at μ_{opt} (top panel in Fig. 16), and it was further confirmed by our calculations with uniform chemical potentials (not shown here). This picture is consistent with the idea that fluctuations between different stripe fillings can help induce SC orders.

Note that, strictly speaking, the SC order should be zero here in a finite-size system since the Hamiltonian does not break (total) particle number conservation without an applied pairing field. However, in the DMRG calculation, the variational ground states often break the symmetry due to the finite bond dimensions kept. This feature has been

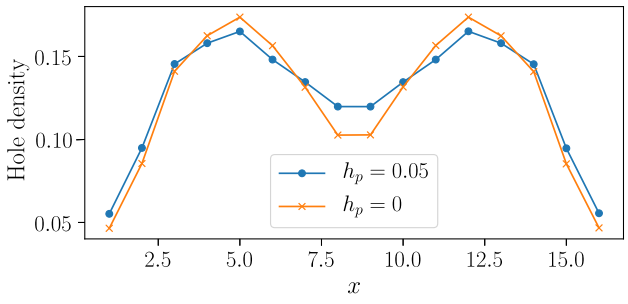

FIG. 15. Comparison of the local hole densities on different rungs for 16×4 systems with $h_p = 0.05$ and with zero pairing field. The system with the pairing field is the same as in Fig. 5 with $\mu = 1.72$.

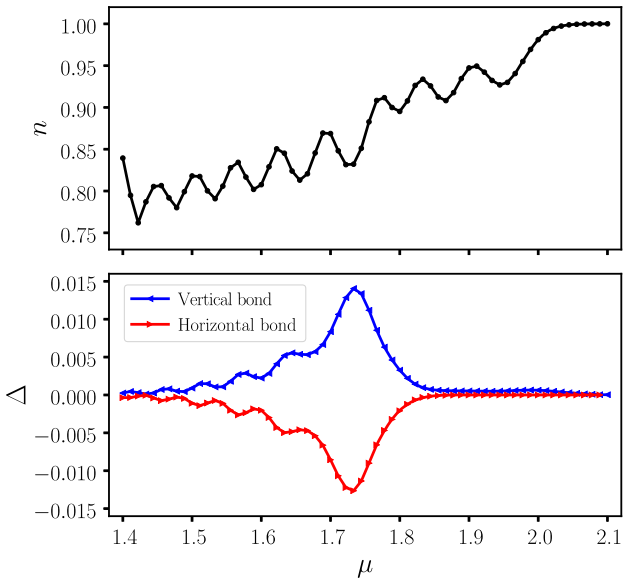

FIG. 16. The system is a 64×4 cylinder with local chemical potential μ linearly changing along the longitudinal direction. (Upper panel) Particle densities along the longitudinal direction. The x axis has been replaced by the local μ on the corresponding position. (Lower panel) The local SC orders on the vertical (blue) and horizontal (red) bonds along the longitudinal direction. The results are obtained by using DMRG without conserving total particle number (grand canonical ensemble).

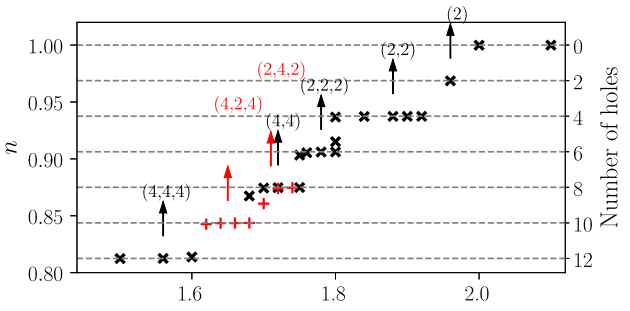

FIG. 17. The density dependence on μ for a 16×4 cylinder with pairing field $h_p = 0.25$ at the left edge. The numbers in the parentheses are the number of holes in each stripe, from left to right. For example, (4,4) means two filled stripes (with four holes). The red color indicates the mixture of different stripe fillings.

used in the past to study the magnetization and now the SC pairing order.

In Fig. 17, we show the particle density (number of holes) as a function of chemical potential μ for a 16×4 cylinder with pinning pairing field $h_p = 0.25$ at the left edge. The density is consistent with the local density in Fig. 16, confirming the reliability of the analysis. The number of holes in each stripe is shown in parentheses. Note that the number of holes in a stripe is even for all μ. This result indicates that, although there is no long-range SC order as we conclude in the main text, short-range pairing exists in the stripes.

APPENDIX D: FILLED AND 2/3-FILLED STRIPES ON SIX-LEG CYLINDERS

Besides the filled stripes, we also considered the 2/3-filled stripes on width-six cylinders. The filled and 2/3-filled stripes are the only two striped states that can be stabilized on width-six cylinders in DMRG. In Fig. 18, we show the pair-pair correlations for the 2/3-filled stripes on a 48×6 system. The correlations for both the finite bond dimension m and the infinite m are shown. The detail of the extrapolation will be shown in the next section. Both the power-law and the exponential fittings are shown. As in the filled stripes, the correlations decay exponentially with distance. The inset shows the absolute values of the correlations on both the vertical bonds and the horizontal bonds. The correlations on the horizontal bonds again are perfectly symmetric with the vertical bonds at the same location but with opposite sign, consistent with the d-wave symmetry.

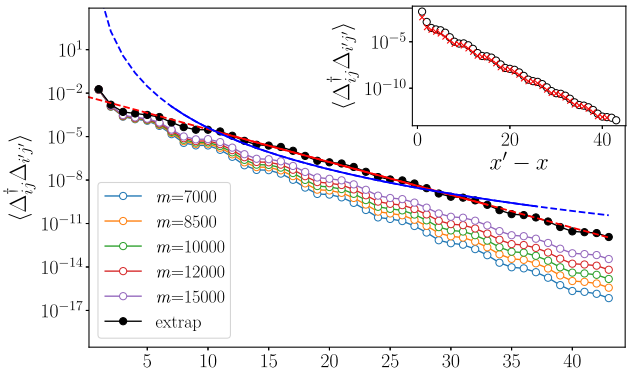

FIG. 18. SC pair-pair correlation for the 2/3-filled stripes with 1/8 hole doping on 48×6 cylinders. Different curves are for different bond dimensions m, as well as the extrapolation to the infinite bond dimension. The pair separation $(x_0 - x)$ is measured with respect to the reference bond, a vertical bond at $x = 5$. Both exponential (red line) and algebraic (blue curve) fits are shown; solid (dashed) region indicates the region (not) used in the fits. The correlation length is approximately 1.9 from the fitting. The inset shows the (negative) correlations on the vertical (‖) [horizontal (⊥)] bonds for $m = 15\,000$.

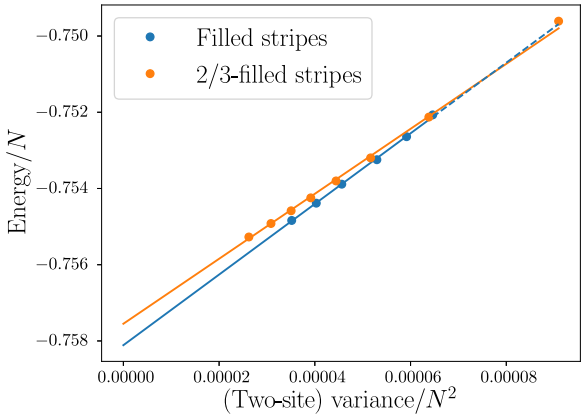

FIG. 19. Linear extrapolation of ground-state energy with the two-site energy variances for the filled and the 2/3-filled stripes on 48×6 cylinders. The MPS bond dimensions shown for the filled stripes are from 8500 to 22 000, and for the 2/3-filled stripes, they are from 7000 to 15 000. The extrapolated energy is $-0.7581(6)$ for the filled stripes and $-0.7574(4)$ for the 2/3-filled stripes.

In Fig. 19, we show the linear extrapolation of the energies with the two-site variance for both the filled and the 2/3-filled stripes. The clearly linear behaviors typically indicate the stability of the MPS toward the zero-variance limit. In other words, the MPS basically stays in the same state for the considered bond dimensions. The crossing of the lines shows that the filled stripes are lower in energy only when the bond dimension is sufficiently large. The filled stripes need larger bond dimension than the 2/3-filled stripes to achieve the same variance because it contains higher entanglement.

APPENDIX E: PAIR-PAIR CORRELATION EXTRAPOLATIONS

Here, we discuss some details of the DMRG simulations. In the simulations preserving $SU(2)$ symmetry, i.e., the simulations on the systems without any pairing field, temporary local chemical potentials are applied in the first few sweeps on the expected locations of the stripes to stabilize the states and improve convergence. One often also applies the magnetic pinning field to stabilize the stripes; however, in our cases, the magnetic field will break the $SU(2)$ symmetry, so no magnetic pinning field is used. For the filled and the 2/3-filled stripes, the temporary chemical potentials are applied up to $m = 4000$ ($m = 1400$), and then they are switched off for the further sweeps of larger m.

For the same systems, the single-site update is used in DMRG. To eliminate the finite bond-dimension effect, we employ the extrapolations of physical quantities (for example, energy and pair-pair correlations) with the two-site energy variances [88]. In two-site DMRG, one usually extrapolates the physical quantities with the so-called

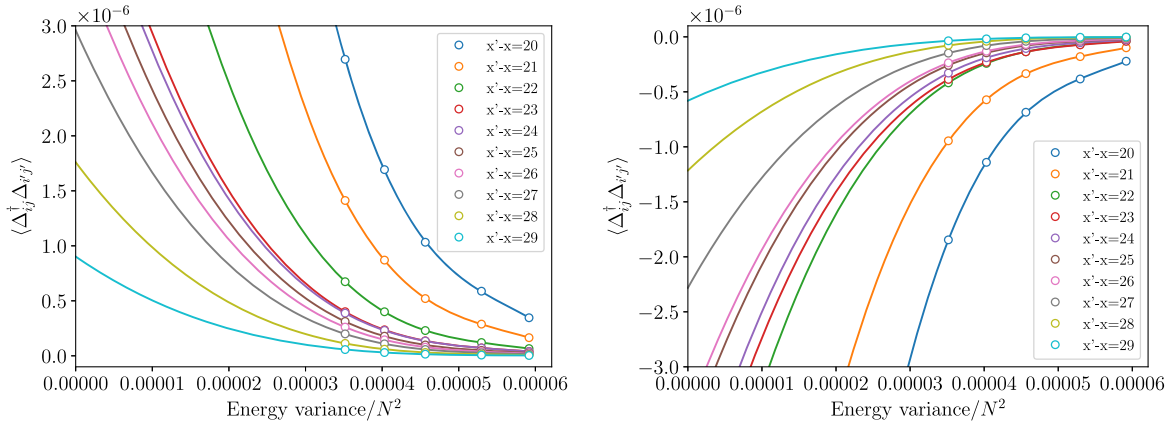

FIG. 20. Pair-pair correlations (dots) and the cubic extrapolations (curves) using the two-site variance on the vertical bonds (left panel) and the horizontal bonds (right panel). The reference bond is the vertical bond on $x = 5$. The system consists of the filled stripes on a 48×6 cylinder as in Fig. 7. The MPS bond dimensions m are from 10 000 to 22 000.

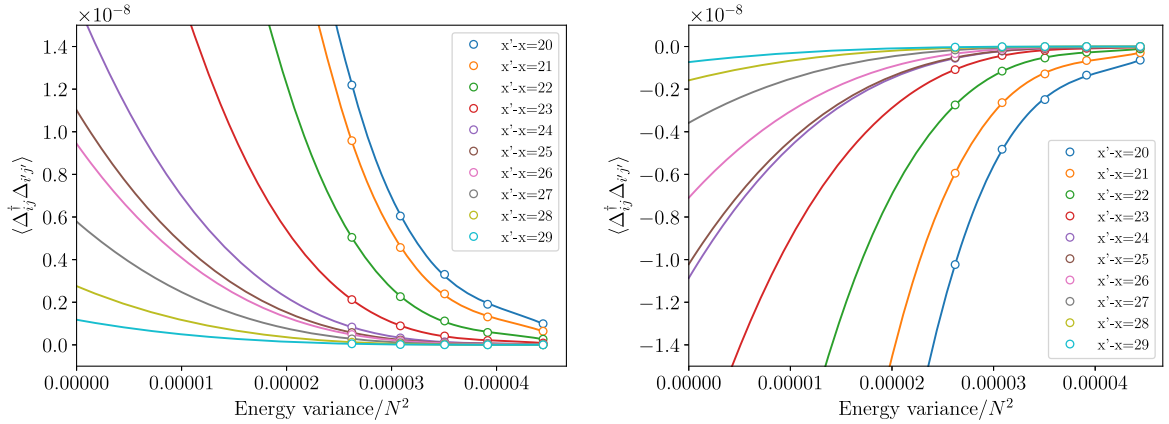

FIG. 21. Pair-pair correlations (dots) and the cubic extrapolations (curves) by the two-site variance on the vertical bonds (left panel) and the horizontal bonds (right panel). The reference bond is the vertical bond on $x = 5$. The system consists of the 2/3-filled stripes on a 48×6 cylinder as in Fig. 18. The MPS bond dimensions m are from 7000 to 15 000.

truncation error (alternatively called discarded weight). However, in single-site DMRG, the truncation errors are not well defined. Thus, we extrapolate the physical quantities with the two-site energy variance, which is an approximation of the full variance $\langle(\hat{H} - E)^2\rangle/N^2$. Physically, the variance is a perfect quantity to extrapolate with since it measures the distance of the variational state to an eigenstate. In practice, this extrapolation scheme was demonstrated to be as reliable as the extrapolation by the truncation error [88].

At the largest bond dimension we can achieve, which to our knowledge is also the largest bond dimension that has been achieved to date, the pair-pair correlation vs energy variance has not yet reached the linear region. We thus perform cubic extrapolations to best fit the data, as shown in Figs. 20 and 21. Since the correlations on different distances have quite different scales, we show the results only for part of the distance, which is long enough but far enough away from the boundary. Although here we showed only the cubic extrapolations, we also tested other extrapolations—for example, the linear extrapolation of the last three data points. The results are very similar to what is presented, and they lead to the same conclusion (exponential decays).

[1] J. G. Bednorz and K. A. Müller, *Possible High T_c Superconductivity in the Ba-La-Cu-O System*, Z. Phys. B **64**, 189 (1986).
[2] E. Dagotto, *Correlated Electrons in High-Temperature Superconductors*, Rev. Mod. Phys. **66**, 763 (1994).
[3] J. Hubbard, *Electron Correlations in Narrow Energy Bands*, Proc. R. Soc. A **276**, 238 (1963).

[4] P. W. Anderson, *The Resonating Valence Bond State in La_2CuO_4 and Superconductivity*, Science **235**, 1196 (1987).

[5] F. C. Zhang and T. M. Rice, *Effective Hamiltonian for the Superconducting Cu Oxides*, Phys. Rev. B **37**, 3759 (1988).

[6] J. E. Hirsch, *Two-Dimensional Hubbard Model: Numerical Simulation Study*, Phys. Rev. B **31**, 4403 (1985).

[7] E. Vitali, H. Shi, M. Qin, and S. Zhang, *Computation of Dynamical Correlation Functions for Many-Fermion Systems with Auxiliary-Field Quantum Monte Carlo*, Phys. Rev. B **94**, 085140 (2016).

[8] M. Qin, H. Shi, and S. Zhang, *Benchmark Study of the Two-Dimensional Hubbard Model with Auxiliary-Field Quantum Monte Carlo Method*, Phys. Rev. B **94**, 085103 (2016).

[9] D. J. Scalapino, *A Common Thread: The Pairing Interaction for Unconventional Superconductors*, Rev. Mod. Phys. **84**, 1383 (2012).

[10] S. A. Kivelson, E. Fradkin, and V. J. Emery, *Electronic Liquid-Crystal Phases of a Doped Mott Insulator*, Nature (London) **393**, 550 (1998).

[11] E. Fradkin, S. A. Kivelson, and J. M. Tranquada, *Colloquium*, Rev. Mod. Phys. **87**, 457 (2015).

[12] T. I. Vanhala and P. Törmä, *Dynamical Mean-Field Theory Study of Stripe Order and d-Wave Superconductivity in the Two-Dimensional Hubbard Model*, Phys. Rev. B **97**, 075112 (2018).

[13] H. Yokoyama and H. Shiba, *Variational Monte-Carlo Studies of Superconductivity in Strongly Correlated Electron Systems*, J. Phys. Soc. Jpn. **57**, 2482 (1988).

[14] C. Gros, *Superconductivity in Correlated Wave Functions*, Phys. Rev. B **38**, 931 (1988).

[15] D. Poilblanc, J. Riera, and E. Dagotto, *d-Wave Bound State of Holes in an Antiferromagnet*, Phys. Rev. B **49**, 12318 (1994).

[16] A. I. Lichtenstein and M. I. Katsnelson, *Antiferromagnetism and d-Wave Superconductivity in Cuprates: A Cluster Dynamical Mean-Field Theory*, Phys. Rev. B **62**, R9283 (2000).

[17] S. Sorella, G. B. Martins, F. Becca, C. Gazza, L. Capriotti, A. Parola, and E. Dagotto, *Superconductivity in the Two-Dimensional t-J Model*, Phys. Rev. Lett. **88**, 117002 (2002).

[18] T. A. Maier, M. Jarrell, T. C. Schulthess, P. R. C. Kent, and J. B. White, *Systematic Study of d-Wave Superconductivity in the 2D Repulsive Hubbard Model*, Phys. Rev. Lett. **95**, 237001 (2005).

[19] D. Sénéchal, P.-L. Lavertu, M.-A. Marois, and A.-M. S. Tremblay, *Competition between Antiferromagnetism and Superconductivity in High-T_c Cuprates*, Phys. Rev. Lett. **94**, 156404 (2005).

[20] M. Capone and G. Kotliar, *Competition between d-Wave Superconductivity and Antiferromagnetism in the Two-Dimensional Hubbard Model*, Phys. Rev. B **74**, 054513 (2006).

[21] M. Aichhorn, E. Arrigoni, M. Potthoff, and W. Hanke, *Variational Cluster Approach to the Hubbard Model: Phase-Separation Tendency and Finite-Size Effects*, Phys. Rev. B **74**, 235117 (2006).

[22] M. Lugas, L. Spanu, F. Becca, and S. Sorella, *Finite Compressibility in the Low-Doping Region of the Two-Dimensional t-J Model*, Phys. Rev. B **74**, 165122 (2006).

[23] T. Aimi and M. Imada, *Does Simple Two-Dimensional Hubbard Model Account for High-T_c Superconductivity in Copper Oxides?*, J. Phys. Soc. Jpn. **76**, 113708 (2007).

[24] H. Yokoyama, M. Ogata, and Y. Tanaka, *Mott Transitions and d-Wave Superconductivity in Half-Filled-Band Hubbard Model on Square Lattice with Geometric Frustration*, J. Phys. Soc. Jpn. **75**, 114706 (2006).

[25] M. Yokoyama, H. Amitsuka, S. Itoh, I. Kawasaki, K. Tenya, and H. Yoshizawa, *Neutron Scattering Study on Competition between Hidden Order and Antiferromagnetism in $U(Ru_{1-x}Rh_x)_2Si_2$ ($x \leq 0.05$)*, J. Phys. Soc. Jpn. **73**, 545 (2004).

[26] D. Eichenberger and D. Baeriswyl, *Superconductivity and Antiferromagnetism in the Two-Dimensional Hubbard Model: A Variational Study*, Phys. Rev. B **76**, 180504(R) (2007).

[27] A. Macridin, M. Jarrell, and T. Maier, *Phase Separation in the Hubbard Model Using the Dynamical Cluster Approximation*, Phys. Rev. B **74**, 085104 (2006).

[28] W.-J. Hu, F. Becca, and S. Sorella, *Absence of Static Stripes in the Two-Dimensional t-J Model Determined Using an Accurate and Systematic Quantum Monte Carlo Approach*, Phys. Rev. B **85**, 081110(R) (2012).

[29] E. Gull and A. J. Millis, *Energetics of Superconductivity in the Two-Dimensional Hubbard Model*, Phys. Rev. B **86**, 241106(R) (2012).

[30] E. Gull, O. Parcollet, and A. J. Millis, *Superconductivity and the Pseudogap in the Two-Dimensional Hubbard Model*, Phys. Rev. Lett. **110**, 216405 (2013).

[31] X. Chen, J. P. F. LeBlanc, and E. Gull, *Superconducting Fluctuations in the Normal State of the Two-Dimensional Hubbard Model*, Phys. Rev. Lett. **115**, 116402 (2015).

[32] T. Misawa and M. Imada, *Origin of High-T_c Superconductivity in Doped Hubbard Models and Their Extensions: Roles of Uniform Charge Fluctuations*, Phys. Rev. B **90**, 115137 (2014).

[33] B.-X. Zheng and G. K.-L. Chan, *Ground-State Phase Diagram of the Square Lattice Hubbard Model from Density Matrix Embedding Theory*, Phys. Rev. B **93**, 035126 (2016).

[34] A. S. Darmawan, Y. Nomura, Y. Yamaji, and M. Imada, *Stripe and Superconducting Order Competing in the Hubbard Model on a Square Lattice Studied by a Combined Variational Monte Carlo and Tensor Network Method*, Phys. Rev. B **98**, 205132 (2018).

[35] S. Zhang, J. Carlson, and J. E. Gubernatis, *Pairing Correlations in the Two-Dimensional Hubbard Model*, Phys. Rev. Lett. **78**, 4486 (1997).

[36] M. Guerrero, G. Ortiz, and J. E. Gubernatis, *Correlated Wave Functions and the Absence of Long-Range Order in Numerical Studies of the Hubbard Model*, Phys. Rev. B **59**, 1706 (1999).

[37] C. T. Shih, Y. C. Chen, H. Q. Lin, and T. K. Lee, *d-Wave Pairing Correlation in the Two-Dimensional t-J Model*, Phys. Rev. Lett. **81**, 1294 (1998).

[38] Y.-F. Jiang, J. Zaanen, T. P. Devereaux, and H.-C. Jiang, *Ground State Phase Diagram of the Doped Hubbard Model on the 4-Leg Cylinder*, arXiv:1907.11728.

[39] K. Machida, *Magnetism in La_2CuO_4 Based Compounds*, Physica C **158**, 192 (1989).

[40] J. Zaanen and O. Gunnarsson, *Charged Magnetic Domain Lines and the Magnetism of High-T_c Oxides*, Phys. Rev. B **40**, 7391 (1989).

[41] M. Kato, K. Machida, H. Nakanishi, and M. Fujita, *Soliton Lattice Modulation of Incommensurate Spin Density Wave in Two Dimensional Hubbard Model—A Mean Field Study*, J. Phys. Soc. Jpn. **59**, 1047 (1990).

[42] D. Poilblanc and T. M. Rice, *Charged Solitons in the Hartree-Fock Approximation to the Large-U Hubbard Model*, Phys. Rev. B **39**, 9749 (1989).

[43] H. J. Schulz, *Domain Walls in a Doped Antiferromagnet*, J. Phys. France **50**, 2833 (1989).

[44] S. R. White and D. J. Scalapino, *Density Matrix Renormalization Group Study of the Striped Phase in the 2D t-J Model*, Phys. Rev. Lett. **80**, 1272 (1998).

[45] S. R. White and D. J. Scalapino, *Competition between Stripes and Pairing in a $t-t'-j$ Model*, Phys. Rev. B **60**, R753 (1999).

[46] A. Himeda, T. Kato, and M. Ogata, *Stripe States with Spatially Oscillating d-Wave Superconductivity in the Two-Dimensional $t-t'-J$ Model*, Phys. Rev. Lett. **88**, 117001 (2002).

[47] S. R. White and D. J. Scalapino, *Stripes on a 6-Leg Hubbard Ladder*, Phys. Rev. Lett. **91**, 136403 (2003).

[48] G. Hager, G. Wellein, E. Jeckelmann, and H. Fehske, *Stripe Formation in Doped Hubbard Ladders*, Phys. Rev. B **71**, 075108 (2005).

[49] M. Raczkowski, M. Capello, D. Poilblanc, R. Frésard, and A. M. Oleś, *Unidirectional d-Wave Superconducting Domains in the Two-Dimensional t-J Model*, Phys. Rev. B **76**, 140505(R) (2007).

[50] C.-P. Chou, N. Fukushima, and T. K. Lee, *Cluster-Glass Wave Function in the Two-Dimensional Extended t-J Model*, Phys. Rev. B **78**, 134530 (2008).

[51] C.-C. Chang and S. Zhang, *Spin and Charge Order in the Doped Hubbard Model: Long-Wavelength Collective Modes*, Phys. Rev. Lett. **104**, 116402 (2010).

[52] P. Corboz, S. R. White, G. Vidal, and M. Troyer, *Stripes in the Two-Dimensional t-J Model with Infinite Projected Entangled-Pair States*, Phys. Rev. B **84**, 041108(R) (2011).

[53] P. Corboz, T. M. Rice, and M. Troyer, *Competing States in the t-J Model: Uniform d-Wave State versus Stripe State*, Phys. Rev. Lett. **113**, 046402 (2014).

[54] H.-H. Zhao, K. Ido, S. Morita, and M. Imada, *Variational Monte Carlo Method for Fermionic Models Combined with Tensor Networks and Applications to the Hole-Doped Two-Dimensional Hubbard Model*, Phys. Rev. B **96**, 085103 (2017).

[55] G. Ehlers, S. R. White, and R. M. Noack, *Hybrid-Space Density Matrix Renormalization Group Study of the Doped Two-Dimensional Hubbard Model*, Phys. Rev. B **95**, 125125 (2017).

[56] H.-C. Jiang and T. P. Devereaux, *Superconductivity in the Doped Hubbard Model and Its Interplay with Next-Nearest Hopping t'*, Science **365**, 1424 (2019).

[57] B. Ponsioen, S. S. Chung, and P. Corboz, *Period 4 Stripe in the Extended Two-Dimensional Hubbard Model*, Phys. Rev. B **100**, 195141 (2019).

[58] O. K. Andersen, A. I. Liechtenstein, O. Jepsen, and F. Paulsen, *LDA Energy Bands, Low-Energy Hamiltonians, t', t'', $t_\perp$ (k), and $J_\perp$*, J. Phys. Chem. Solids **56**, 1573 (1995).

[59] E. Cocchi, L. A. Miller, J. H. Drewes, M. Koschorreck, D. Pertot, F. Brennecke, and M. Köhl, *Equation of State of the Two-Dimensional Hubbard Model*, Phys. Rev. Lett. **116**, 175301 (2016).

[60] P. T. Brown, D. Mitra, E. Guardado-Sanchez, R. Nourafkan, A. Reymbaut, C.-D. Hébert, S. Bergeron, A.-M. S. Tremblay, J. Kokalj, D. A. Huse, P. Schauß, and W. S. Bakr, *Bad Metallic Transport in a Cold Atom Fermi-Hubbard System*, Science **363**, 379 (2019).

[61] A. Mazurenko, C. S. Chiu, G. Ji, M. F. Parsons, M. Kanász-Nagy, R. Schmidt, F. Grusdt, E. Demler, D. Greif, and M. Greiner, *A Cold-Atom Fermi-Hubbard Antiferromagnet*, Nature (London) **545**, 462 (2017).

[62] J. Koepsell, J. Vijayan, P. Sompet, F. Grusdt, T. A. Hilker, E. Demler, G. Salomon, I. Bloch, and C. Gross, *Imaging Magnetic Polarons in the Doped Fermi-Hubbard Model*, Nature (London) **572**, 358 (2019).

[63] B.-X. Zheng, C.-M. Chung, P. Corboz, G. Ehlers, M.-P. Qin, R. M. Noack, H. Shi, S. R. White, S. Zhang, and G. K.-L. Chan, *Stripe Order in the Underdoped Region of the Two-Dimensional Hubbard Model*, Science **358**, 1155 (2017).

[64] Z. Guguchia, A. Maisuradze, G. Ghambashidze, R. Khasanov, A. Shengelaya, and H. Keller, *Tuning the Static Spin-Stripe Phase and Superconductivity in* $La_{2-x}Ba_xCuO_4$ *($x = 1/8$) by Hydrostatic Pressure*, New J. Phys. **15**, 093005 (2013).

[65] J. M. Tranquada, G. D. Gu, M. Hücker, Q. Jie, H.-J. Kang, R. Klingeler, Q. Li, N. Tristan, J. S. Wen, G. Y. Xu, Z. J. Xu, J. Zhou, and M. v. Zimmermann, *Evidence for Unusual Superconducting Correlations Coexisting with Stripe Order in* $La_{1.875}Ba_{0.125}CuO_4$, Phys. Rev. B **78**, 174529 (2008).

[66] M. Hücker, M. v. Zimmermann, G. D. Gu, Z. J. Xu, J. S. Wen, G. Xu, H. J. Kang, A. Zheludev, and J. M. Tranquada, *Stripe Order in Superconducting* $La_{2-x}Ba_xCuO_4$ *($0.095 \leq x \leq 0.155$)*, Phys. Rev. B **83**, 104506 (2011).

[67] M. Miyazaki, K. Yamaji, and T. Yanagisawa, *Possible Coexistence of Superconductivity and Static SDW Stripes in the Two-Dimensional Hubbard Model*, J. Phys. Chem. Solids **63**, 1403 (2002).

[68] S. J. Wetzel, *Exploring the Hubbard Model on the Square Lattice at Zero Temperature with a Bosonized Functional Renormalization Approach*, arXiv:1712.04297.

[69] S. Zhang, J. Carlson, and J. E. Gubernatis, *Constrained Path Monte Carlo Method for Fermion Ground States*, Phys. Rev. B **55**, 7464 (1997).

[70] M. Qin, H. Shi, and S. Zhang, *Coupling Quantum Monte Carlo and Independent-Particle Calculations: Self-Consistent Constraint for the Sign Problem Based on the Density or the Density Matrix*, Phys. Rev. B **94**, 235119 (2016).

[71] S. R. White, *Density Matrix Formulation for Quantum Renormalization Groups*, Phys. Rev. Lett. **69**, 2863 (1992).

[72] A. V. Chubukov and J. P. Lu, *Pairing Instabilities in the Two-Dimensional Hubbard Model*, Phys. Rev. B **46**, 11163 (1992).

[73] A. V. Chubukov, *Kohn-Luttinger Effect and the Instability of a Two-Dimensional Repulsive Fermi Liquid at $T = 0$*, Phys. Rev. B **48**, 1097 (1993).

[74] M. Jarrell, T. Maier, M. H. Hettler, and A. N. Tahvildarzadeh, *Phase Diagram of the Hubbard Model: Beyond the Dynamical Mean Field*, Europhys. Lett. **56**, 563 (2001).

[75] S. Raghu, S. A. Kivelson, and D. J. Scalapino, *Superconductivity in the Repulsive Hubbard Model: An Asymptotically Exact Weak-Coupling Solution*, Phys. Rev. B **81**, 224505 (2010).

[76] Y. Deng, E. Kozik, N. V. Prokof'ev, and B. V. Svistunov, *Emergent BCS Regime of the Two-Dimensional Fermionic Hubbard Model: Ground-State Phase Diagram*, Europhys. Lett. **110**, 57001 (2015).

[77] S. R. White and A. L. Chernyshev, *Neél Order in Square and Triangular Lattice Heisenberg Models*, Phys. Rev. Lett. **99**, 127004 (2007).

[78] E. Y. Loh, J. E. Gubernatis, R. T. Scalettar, S. R. White, D. J. Scalapino, and R. L. Sugar, *Sign Problem in the Numerical Simulation of Many-Electron Systems*, Phys. Rev. B **41**, 9301 (1990).

[79] C.-C. Chang and S. Zhang, *Spatially Inhomogeneous Phase in the Two-Dimensional Repulsive Hubbard Model*, Phys. Rev. B **78**, 165101 (2008).

[80] H. Shi and S. Zhang, *Many-Body Computations by Stochastic Sampling in Hartree-Fock-Bogoliubov Space*, Phys. Rev. B **95**, 045144 (2017).

[81] E. Vitali, P. Rosenberg, and S. Zhang, *Calculating Ground-State Properties of Correlated Fermionic Systems with BCS Trial Wave Functions in Slater Determinant Path-Integral Approaches*, Phys. Rev. A **100**, 023621 (2019).

[82] S. R. White, *Density-Matrix Algorithms for Quantum Renormalization Groups*, Phys. Rev. B **48**, 10345 (1993).

[83] U. Schollwöck, *The Density-Matrix Renormalization Group in the Age of Matrix Product States*, Ann. Phys. (Amsterdam) **326**, 96 (2011), Special Issue.

[84] E. M. Stoudenmire and S. R. White, *Studying Two-Dimensional Systems with the Density Matrix Renormalization Group*, Annu. Rev. Condens. Matter Phys. **3**, 111 (2012).

[85] C. Hubig, F. Lachenmaier, N.-O. Linden, T. Reinhard, L. Stenzel, A. Swoboda, and M. Grundner, The SYTEN Toolkit.

[86] C. Hubig, Symmetry-Protected Tensor Networks, Ph.D. thesis, LMU München, 2017.

[87] C. Hubig, I. P. McCulloch, U. Schollwöck, and F. A. Wolf, *Strictly Single-Site DMRG Algorithm with Subspace Expansion*, Phys. Rev. B **91**, 155115 (2015).

[88] C. Hubig, J. Haegeman, and U. Schollwöck, *Error Estimates for Extrapolations with Matrix-Product States*, Phys. Rev. B **97**, 045125 (2018).

[89] S. R. White and D. J. Scalapino, *Pairing on Striped $t - t' - j$ Lattices*, Phys. Rev. B **79**, 220504(R) (2009).

[90] S. R. White, D. J. Scalapino, R. L. Sugar, N. E. Bickers, and R. T. Scalettar, *Attractive and Repulsive Pairing Interaction Vertices for the Two-Dimensional Hubbard Model*, Phys. Rev. B **39**, 839 (1989).

[91] D. J. Scalapino, *Superconductivity and Spin Fluctuations*, J. Low Temp. Phys. **117**, 179 (1999).

[92] J. P. F. LeBlanc *et al.* (Simons Collaboration on the Many-Electron Problem), *Solutions of the Two-Dimensional Hubbard Model: Benchmarks and Results from a Wide Range of Numerical Algorithms*, Phys. Rev. X **5**, 041041 (2015).

[93] J. F. Dodaro, H.-C. Jiang, and S. A. Kivelson, *Intertwined Order in a Frustrated Four-Leg t-J Cylinder*, Phys. Rev. B **95**, 155116 (2017).

[94] M. Dolfi, B. Bauer, S. Keller, and M. Troyer, *Pair Correlations in Doped Hubbard Ladders*, Phys. Rev. B **92**, 195139 (2015).

[95] J. M. Tranquada, B. J. Sternlieb, J. D. Axe, Y. Nakamura, and S. Uchida, *Evidence for Stripe Correlations of Spins and Holes in Copper Oxide Superconductors*, Nature (London) **375**, 561 (1995).

[96] P. Rosenberg, H. Shi, and S. Zhang, *Accurate Computations of Rashba Spin-Orbit Coupling in Interacting Systems: From the Fermi Gas to Real Materials*, J. Phys. Chem. Solids **128**, 161 (2019).